JOURNAL OF THERMOPHYSICS AND HEAT TRANSFER
Vol. 21, No. 4, October–December 2007

Laser-Sustained Plasma in a Sonic Nozzle Probed by Fast Atom Beam

K. Amic* and A. Lebéhot†
Centre National de la Recherche Scientifique, 45071 Orléans, France
and
J. D. Parisse‡
Institut Universitaire des Systèmes Thermiques Industriels, 13453 Marseille, France

DOI: 10.2514/1.29306

The plasma sustained by an infrared laser, upstream of a sonic nozzle, is used for the generation of a supersonic freejet. Through a skimmer, a fast atom beam is extracted from the axial part of the freejet final stage, inside the zone of silence. In these conditions, the kinetic properties achieved at the end of the expansion are conserved in the atom beam and reflected in its velocity distribution. As the expansion of the freejet is closely described by the classical isentropic laws, at least on the axis, an equivalent stagnation temperature can be deduced from the time-of-flight velocity distribution of the atom beam. In the same way, the axial velocity at the nozzle throat can be obtained from the mean velocity of the atom beam. Also, the temperature and velocity fields of the plasma are calculated with fluid dynamic models, in the flowfield of the sonic nozzle. Two different solving procedures, including the laser beam energy absorption process, are presented. The values of equivalent stagnation temperature and the axial velocity at the nozzle throat, directly issued from these calculations, are found to be in reasonable agreement with the experimental results.

Nomenclature

C_p = specific heat at constant pressure
D^* = nozzle orifice diameter
$\mathrm{d}S$ = surface element
k = Boltzmann constant
m = atom mass
n = number density
p_0 = stagnation pressure
p_1 = pressure in expansion chamber
$p_{2\text{–}4}$ = pressures in chambers 2–4
$S_{//}$ = speed ratio
T = local translational temperature
$T_{//\infty}$ = final longitudinal translational temperature
T^*_{ax} = axial translational temperature at the nozzle throat
T_e = electron temperature
$T_{\max}$ = maximum of an imposed Gaussian temperature distribution
T_0 = equivalent stagnation temperature
v = flow velocity
v^*_{ax} = axial velocity at the nozzle throat (sonic velocity)
v_∞ = flow velocity at the end of the expansion
W = laser beam power
z = axial distance from laser waist, or from nozzle throat in the cold gas case
z_{freeze} = distance between freezing point and nozzle throat
z_M = distance between Mach disk and nozzle throat
z_w = distance between laser waist and outer wall of the nozzle
γ = ratio of specific heats
Δr = calculation step for radial coordinate

Received 14 December 2006; revision received 21 February 2007; accepted for publication 21 February 2007.

*Ph.D. Student, Laboratoire d'Aérothermique, Centre National de la Recherche Scientifique, 1C Avenue de la Recherche Scientifique, 45071 Orléans, France.

†Research Engineer; currently Institut de Combustion, Aérothermique, Réactivité, Environnement, Centre National de la Recherche Scientifique, 1C Avenue de la Recherche Scientifique, 45071 Orléans, France; lebehot@cnrs-orleans.fr.

‡Associate Professor, Institut Universitaire des Systèmes Thermiques Industriels, Unité Mixte de Recherche 6595, 5 Rue Enrico Fermi, 13453 Marseille, France; JD.Parisse@iut.univ-evry.fr.

I. Introduction

THE fast atom beam extracted from a laser-sustained plasma freejet has axial velocity distributions in quite good agreement with the usual Maxwellian distribution, solution of the Boltzmann equation for the expansion [1]. Also, this distribution is consistent with the model of a virtual neutral gas in isentropic expansion from stagnation conditions T_0, p_0 [2]. So, in spite of very strong gradients in density, temperature, and velocity, in the vicinity of the laser waist and near the nozzle throat, the expansion of the plasma behaves as if it were produced from a neutral perfect gas in equilibrium in the nozzle reservoir with uniform temperature T_0 and uniform pressure p_0. This means that the plasma relaxation processes do not affect the translational behavior of the heavy particles (atoms and ions) in the freejet. This is consistent with the low ionization degrees achieved downstream of the nozzle [3]. In a simple one-dimensional schematic description of the expansion [3–5], it has been assumed that electrons and heavy particles are locally in thermal equilibrium inside the nozzle reservoir, whereas heavy particle translational temperature and electron temperature begin to part from each other at the very beginning of the expansion. The assumption of a single local equilibrium temperature inside the nozzle reservoir is rather correct, mainly in the vicinity of the plasma core [6]. Anyway, T_0 is only defined as the uniform stagnation temperature of a gas in isentropic expansion which would give the same velocity distribution as obtained from the real plasma. Then, the atom beam can be considered as a probe able to report about the properties of the plasma, inside the nozzle, where no other experimental diagnosis is available. And so, it is possible to compare the value of T_0, as obtained experimentally from time-of-flight measurements, with the axial temperature calculated at the nozzle throat, using the isentropic law [1]

$$T_0 = T^*_{\mathrm{ax}}\left(1 + \frac{\gamma - 1}{2}\right) \tag{1}$$

where the specific heat ratio is assumed to be constant: 5/3 for monatomic gas. In the same way, the measured mean velocity of the atom beam is the final longitudinal velocity achieved at the end of the expansion, which is related to the axial velocity at the nozzle throat by the law of adiabatic expansion [1]:

$$v_\infty \approx \sqrt{\frac{\gamma+1}{\gamma-1}} v_{\mathrm{ax}}^* = 2 v_{\mathrm{ax}}^* \tag{2}$$

The goal of this paper is to present calculation procedures for the description of the temperature, density, and velocity fields, upstream of the nozzle, and in the freejet expansion, as far as possible. The calculations are first checked without laser power, for a neutral gas expanding at room temperature. In this case, the usual axial isentropic laws should be obtained very accurately, even upstream of the nozzle throat, as often observed experimentally [7]. After validation of the calculation through these flow predictions, the laser power is added for a complete description of the plasma. Experimental and theoretical values of T_0 and v_{ax}^* can then be compared.

It is of interest to notice that the spot where the properties are compared is reached by a backward procedure, starting far downstream of the nozzle, for the experimental measurement (the flight length is longer than 4 m), and by a forward procedure, from inside the nozzle, for the theoretical calculation.

II. Experimental Conditions

The experimental device and the experimental procedures have been described previously [2–5]. Only the characteristics necessary for the understanding of the present work are recalled here. Gas mixtures Ar-O_2 of various concentrations [4,5] have been used, but pure argon is here taken for the sake of simplicity of the interpretations. A freejet is generated from a sonic nozzle (circular diameter of $D^* = 0.5$ mm in a plane thin wall of thickness 0.5 mm). An infrared laser beam of wavelength 10.6 μm, propagating along the axis of the nozzle, is focused just upstream of the nozzle throat by means of a ZnSe lens with a focal length of 38.1 mm and an f number = 8 (in Fig. 1, the laser beam is represented by the dashed line and its propagation by the open arrow). The diameter of the laser waist is 0.07 mm. The distance between the laser waist and the outer face of the nozzle wall is 1.3 mm. The gas pressure in the nozzle reservoir can be adjusted below 10^6 Pa. This upper limitation in pressure is related to 1) the pumping flow rate in the expansion chamber (4000 m^3/h at pressure p_1 between 5 and 20 Pa), and 2) the permissible stress in the entrance window of the laser beam. The continuous-wave laser power is adjusted between 165 and 385 W (values actually measured at the plasma location). In these conditions, the laser radiation is absorbed by the gas medium through the inverse bremsstrahlung process (see, for example, [8]), and a plasma is formed around the laser waist. The nozzle is an interchangeable piece, made of brass, protected by water cooling and by the boundary layer of the gas flow. For a typical pressure p_0 of 5×10^5 Pa, the flow rate is about 11 slm (standard liter per minute) without plasma, and 2.5 slm with a laser power of 220 W.

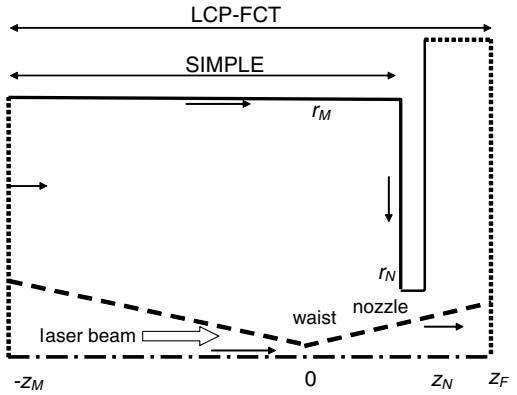

Fig. 1 Calculation region (not to scale).

An atom beam is extracted from the freejet by a skimmer located at a distance z_s of 50–70 mm from the nozzle exit (according to p_0), within the Mach disk location. From hereon, the atom beam crosses three chambers with pressures ranging from 10^{-3} Pa to 10^{-7} Pa, on a distance of 4.17 m. This flight distance is used for the measurement of the velocity distribution of the atom beam. The best Maxwellian analytical fit of this distribution leads to the values of v_∞ and $S_{//}$ (or the translational final temperature) from which is derived the equivalent stagnation temperature through the adiabatic expansion law [1,2]:

$$\frac{1}{2} m v_\infty^2 = \frac{\gamma}{\gamma-1} k (T_0 - T) \tag{3}$$

This formulation is equivalent to Eq. (2) in which T was neglected with respect to T_0 (the measured values of T are between 100 and 400 K). T_0 is not the plasma core temperature, but some intermediate temperature (between the core temperature and the sonic temperature) which is actually expressed by the adiabatic expansion. As it is determined by time-of-flight measurements, this temperature is sometimes called "the time-of-flight temperature" [2,3].

III. Principle of the Calculations

Two different procedures are used:

1) The first model is based on the SIMPLE Patankar procedure (semi-implicit method for pressure-linked equations [9]). This calculation is carried out in the subsonic part, upstream of the nozzle throat, with a homemade calculation code.

2) The second model uses a freely available solver LCP-FCT (Laboratory of Computational Physics: flux corrected transport [10]). This calculation is valid in the supersonic expansion as well as in the nozzle reservoir.

Both models use the general basic system of conservation equations for mass, momentum, and energy, written in cylindrical coordinates [11–14]. Nevertheless, in the SIMPLE procedure, the density conservation equation is disregarded and replaced by a correction of the initial pressure field which minimizes the error made on the mass flow conservation, cell by cell.

Such procedures have often been used previously. Data can be found in the literature for laser-sustained plasmas, as applied to a rocket thruster [11,15], for incompressible flows [16], and, in a much simpler way, for a parallel flowfield, without any radial effect on the velocities [17].

In Table 1, the main characteristics of both calculation procedures are listed and compared. It is worth noticing that the comparison of the computation times is not very significant for the following reasons:

1) LCP-FCT is time integrated; SIMPLE is implemented only in space coordinates and its convergence time depends strongly on the chosen initial conditions.

2) LCP-FCT is carried out with the language FORTRAN FTN77; SIMPLE is written in MATLAB R2006b (The MathWorks, Inc.) with direct imaging of the data. Both calculations are made with a Xeon (Intel) processor with CPU = 3.2 GHz. In these conditions, the total computation times for one set of conditions (p_0, W) are on the order of 12–48 h (between 10^5 and 10^6 time steps for LCP, corresponding to a physical time of about 10^{-4} s, and the same number of space iterations for SIMPLE).

For the LCP-FCT procedure, the time step is adjusted, through the Courant–Friedrichs–Lewy (CFL) number, as a function of local space step and flow velocity. The CFL number has been carefully optimized, according to each situation. In most cases, it is taken equal to 0.01. Also, for LCP, the calculation domain is divided into several parts with different grid properties, to fit at best with the gradients expected in each part. The grid step is small and uniform radially, within the nozzle diameter (Δr smaller than laser waist radius), and axially, inside the nozzle thickness and just in front of the nozzle

Table 1 Compared properties of both calculation procedures

Property	LCP-FCT	SIMPLE
Time dependent	yes	no
Domain of validity	subsonic, supersonic, shock wave	only subsonic part
Viscosity terms	no	yes
Constant specific heats	yes[a]	no, pressure and temperature dependence
Adaptable grid	yes	no[a]
Sonic condition	no	yes, boundary condition
Entrance flow condition	no	yes
Control during computation of convergence speed/stability	yes, controlled time step	no[a], fixed heavy underrelaxation
Relative computation time for the same case (see text)[a]	1	2
Convergence criterion[a]	final axial velocity	conservation of mass flow rate
Grid size (axial × radial)[a]	up to 500 × 500 (stagnation chamber + expansion chamber)	160 × 30 (stagnation chamber only)

[a]Indicates that the limitation is not an intrinsic property of the method, but is rather linked to the present state of the calculation code.

wall. The step increases as a geometrical law toward the outer walls, and toward the inlet and outlet of the domain.

IV. Transport Coefficients

The transport coefficients included in the calculations are written as analytical fits of semi-empirical functions or theoretical data taken from the literature, in terms of pressure and temperature. The temperature range is generally below 25,000 K and the pressure range around 1 atm. The functions are the same as used in [17]. As T_e is not calculated (except in the LCP-FCT nonequilibrium calculation, see Sec. V), it is assumed here that the electron temperature is in equilibrium with the heavy particle temperature. This assumption is not very restrictive in the absorption region [6] where most of the energy exchanges occur (absorption from laser power and radiative losses).

The absorption of the laser beam power is calculated at each axial step, assuming that the beam profile is Gaussian and remains Gaussian in spite of absorption. This assumption seems rather correct, as it has been demonstrated that the shape of the laser beam is not so much affected by the absorption process, which is limited to the vicinity of the laser waist [11,12]. The absorption coefficient is the inverse bremsstrahlung Kramers coefficient [2,18], with the assumption that the prominent effect occurs for collisions between electrons and ions. This latter assumption is valid as far as a high temperature area is imposed for initiating the plasma. This point is discussed in [19,20].

The radiative loss coefficient used is available only at atmospheric pressure. The variation of this coefficient with pressure is then assumed to follow a $p^{3/2}$ law [21].

For the SIMPLE calculation only, when describing the equivalent isentropic expansion, the specific heat at constant pressure is taken as a constant, but, in the equation system, C_P is actually recalculated in each point for the gas of interest [22]. The viscosity is a simple fit of the recommended values derived from collisional integrals [23]. It is noteworthy that the viscosity formulation given in [13] is expected to be better above 15,000 K, due to the effect of Ar^{++} ions, not included in [23]. For the LCP calculation, the specific heat is taken as a constant and the viscosity is disregarded.

V. Initial Conditions

The situation is very different for each model. In the case of a time-dependent calculation (LCP-FCT), each step is expected to be the actual description of a transient process between an initial physical description toward a final stationary state, under the action of a number of constraints which can be put into action one after the other. For the case of a stationary calculation, each step accounts for the numerical convergence from an initial unrealistic system toward its physical stationary state, under the influence of a fixed number of constraints.

For the LCP-FCT calculation, the starting point is the following: both chambers are at the same pressure p_0, and have the same temperature, 300 K, except around the waist of the laser beam, where is applied a narrow Gaussian temperature distribution, with maximum $T_{\max} = 14,000$ K and $1/e$ half-width of order $D^*/2$. At time $t = 0$, the pressure in the expansion chamber is progressively decreased. Simultaneously, the constant-wave laser power is applied (power chosen between 165 and 385 W, the experimental range), together with the pulse of a secondary laser (2×10^5 W during 100 ns). This is the exact description of an experimental procedure for the ignition of the plasma [2–5]. The slow decrease of the pressure in the expansion chamber allows the generation of transient artificial shock waves to be avoided.

The starting conditions are the same for the SIMPLE calculation, limited to the stagnation chamber, and without laser pulse, which is not relevant in stationary conditions.

The Gaussian temperature distribution, which is initially applied, is necessary for the ignition of the plasma by forcing the initial absorption of the laser power by the gas medium. Such an artificial procedure can be avoided by modelling the complete process of plasma ignition [19,20]. This complete model has been carried out here, with the LCP-FCT code, as an optional procedure [24], which will be described in more detail later. Then, the chemistry of the plasma is taken into account, at first with only three species, Ar, Ar^+, and electrons, and introducing a nonequilibrium between the heavy particle and the electron temperatures [6,13]. The plasma is then initiated simply by taking, among initial conditions, a small uniform density of electrons. The absorption coefficient includes then the neutral and ionic parts [19,20]. This extended LCP-FCT process will be called hereafter the "nonequilibrium model."

VI. Boundary Conditions

The boundary conditions in the stagnation chamber are the same for both calculations, and correspond to the experimental conditions: temperature maintained at 300 K on each wall by water cooling (full lines in Fig. 1), vanishing of radial velocities on the outer wall, and of the longitudinal velocities on the front wall (the velocities on boundaries appear as small arrows in Fig. 1). Nevertheless, the size of the test region is taken as much smaller than the experimental stagnation chamber, and is not the same for both calculations (length 20 mm, radius 5 mm in the LCP case, 4 mm and 1.5 mm, respectively, for the SIMPLE case). The goal is obviously to limit the calculation in the smallest volume which surrounds the plasma, without any influence of the walls on the plasma extent. In each case, it has been checked that extending the useful volume over the preceding dimensions does not influence the results significantly.

For the SIMPLE case, it is necessary to take a boundary condition at the nozzle throat, only for enforcing the sonic condition to the system. And so, the longitudinal velocity is imposed equal to the

local sound velocity at the exit of the calculation zone, with the temperature calculated freely by the equation system. Because the exact location of the sonic surface is not known a priori inside the channel of a thick nozzle, the assumption of an infinitely thin wall appears necessary here.

In the expansion chamber, for the LCP-FCT calculation, the boundary is open for the velocities (entrance and exit surfaces are shown by dotted lines in Fig. 1); the values of the other parameters are of little influence on the expansion, as the supersonic process is not affected by the outer conditions. The nozzle wall thickness equals 1 D^*, as in the experimental case.

VII. Test Calculation: Standard Nozzle Reservoir

The complete codes are tested by taking first the laser power equal to zero. The situation is then the case of the standard expansion of a gas from a nozzle reservoir at room temperature. The gas medium is assumed to be homogenous and in equilibrium in the whole volume of the reservoir until the effect of the nozzle begins to take place. Then, the axial variables follow the isentropic rules, which are known to be accurate, even upstream of the nozzle [25], where the Mach number also follows a law of the Ashkenas and Sherman type [7]. It may be noted that, at the high pressures used ($2 \times 10^5 < p_0 < 8 \times 10^5$ Pa), the viscous effects are limited to a very narrow boundary layer which affects very little the paraxial properties of the flow. Furthermore, the step of the space grid may be much larger than the thickness of the boundary layers. Nevertheless, the viscosity is taken into account in the SIMPLE calculation, following [11,13] for the equations, and [23] for the recommended value. For the initial conditions, the pressure and temperature are taken uniform over the whole region (with $T_{\max} = 300$ K), in equilibrium with the wall values.

The final temperature contour map is reported in Fig. 2a, for a stagnation pressure $p_0 = 7 \times 10^5$ Pa in the LCP case. The structure of the freejet appears clearly with a sudden cooling effect, except in the lateral shock wave where the temperature increases again at values higher than 20 K. The isopycnal contours (Fig. 2b) can be compared with those calculated for a very different p_0/p_1 ratio [26]. In the present case, $p_0/p_1 = 70,000$ instead of 17.5 in [26]. This is the reason why the Mach disk is not present in Fig. 2b. It should appear far after the end of the continuous regime (at about 145 D^*), i.e., out of the domain of validity of the present calculation. This limitation does not appear in [26] because the product $p_0 D^*$ is larger than in the present case (750 instead of 350 Pa × m), and therefore also the freezing distance [27].

For the subsonic region, the agreement between SIMPLE and LCP calculations is quite good, provided that the location of the SIMPLE thin nozzle wall is taken slightly inside the thickness of the LCP nozzle, at the location of the sonic plane. This is demonstrated in Fig. 3, in which the axial Mach number and temperature are presented, as a function of axial distance. For comparison, the Ashkenas and Sherman data [7] are also given, obtained for a realistic nozzle of thickness 0.6 D^*. The isentropic law [1,7], calculated for an ideal infinitely thin nozzle, is shown as a dashed-dotted line, and the same, shifted by the nozzle thickness of 1 D^*, as a dashed line. The pressure and axial velocity are given in Fig. 4. The conservation of the mass flow rate along the cross sections of the calculation region is maintained to within 2%, except for the last two points in the SIMPLE scheme, where it can remain at about 10%; this shift accounts for the background lack of convergence. Each result is compared with the axial isentropic curve obtained through the Mach number, as calculated with the usual set of formula [2] used for $z/D^* < 1$ and $z/D^* > 1$, respectively.

The agreement of the results with the isentropic laws is very good for $z/D^* < 0$, and fairly good in the expanded gas, as far as the real thickness of the nozzle is taken into account. It may be noticed that the expansion is very fast, and nearly frozen at a distance of 5 D^*. This is consistent with the scale given by the "sudden freeze model" (assuming a sudden transition from continuous to rarefied flow at some freezing distance z_{freeze}) [27] and a previous one-dimension calculation [3]. And so, not only is the agreement excellent at $z = 0$,

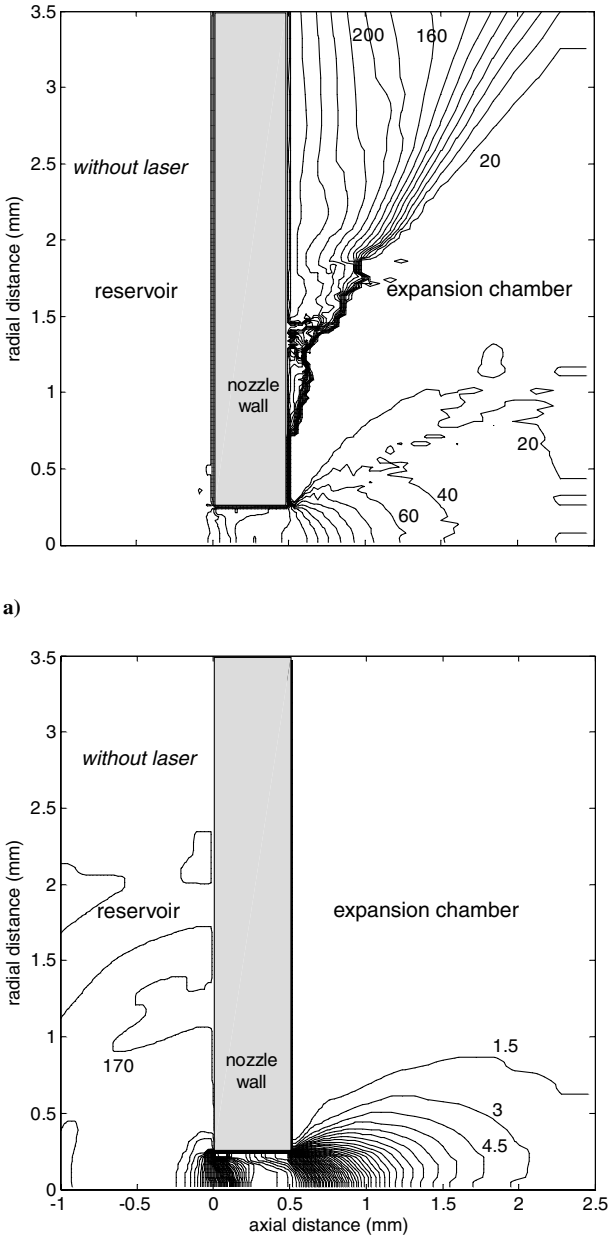

Fig. 2 Contour maps for a) temperature, and b) number density (units in Kelvin and 10^{24} m^{-3}, respectively); $p_0 = 7 \times 10^5$ Pa, $p_1 = 15$ Pa, $W = 0$, LCP-FCT calculation.

but also at the end of the continuous part of the jet. For instance, the final velocity is found to be about 540 ms^{-1} instead of 555 ms^{-1} obtained experimentally (provided that condensation effects are avoided) (see, for example, [28,29]), as well as by the isentropic law. Figure 5 summarizes the different scales of interest for this interpretation, and a number of typical values are given in Table 2 (where italic type corresponds to calculated values). The Mach disk distance is estimated by assuming valid the usual relation [7] $z_M = 0.67 \times (p_0/p_1)^{1/2}$ in spite of nonuniform pressure and temperature in the plasma/nozzle region. This relation is consistent with the direct visual estimation as well as with the optimized distance of the skimmer.

This general agreement on the axis does not necessarily mean that the results are correct in the whole volume, but, as neither artifact nor accident appears anywhere, and as the mass flow rate is well conserved through any cross section of the test region, it can be expected that the flow properties are well predicted by the present calculations.

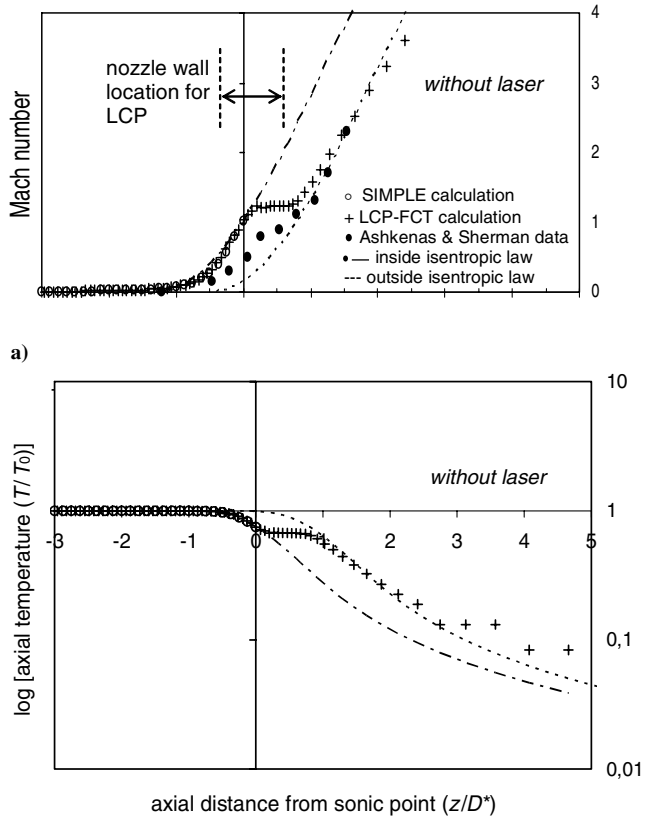

Fig. 3 Calculated laws for a) axial Mach number, and b) temperature; $p_0 = 7 \times 10^5$ Pa, $p_1 = 15$ Pa, $W = 0$.

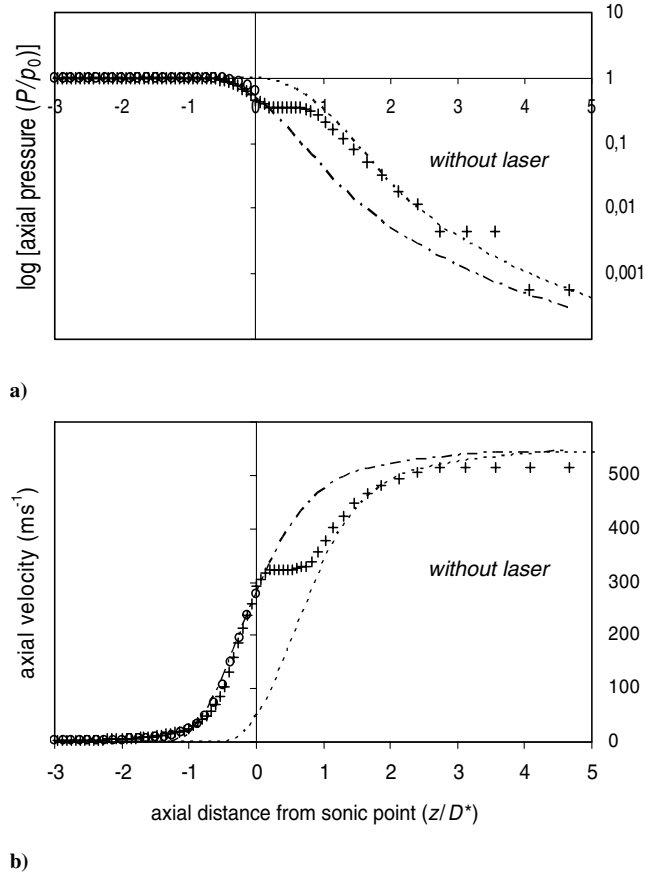

Fig. 4 Same as Fig. 3 for a) pressure, and b) velocity.

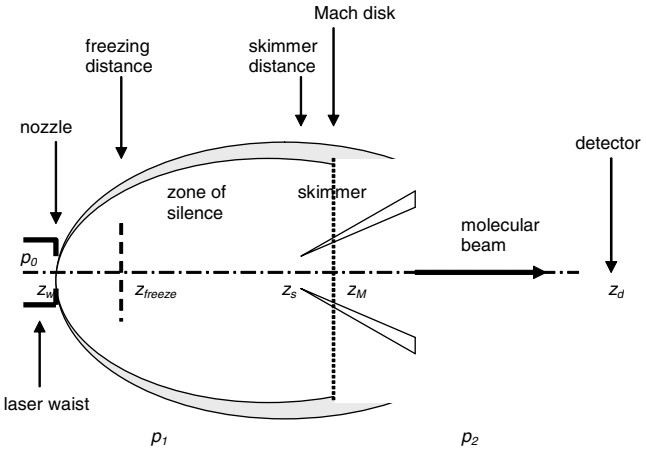

Fig. 5 Scheme of the experimental setup (not to scale).

And so, the laser beam power can be added safely as the energy source in the flow equations.

VIII. Complete Calculation: Laser-Sustained Plasma in the Flowfield of the Nozzle

The boundary conditions are the same as those of the standard case, without laser power, because of the water cooling of the walls. It is always checked, in each calculation, that the plasma effects do not reach the vicinity of the boundaries (if otherwise, the boundaries should be enlarged). Then, only three changes have to be introduced in the calculation to maintain the plasma:

1) Laser power is taken as a realistic value in the range obtained experimentally for the maintenance of the plasma ("effective" laser power, i.e., power actually available for the plasma after losses along the optical path).

2) The maximum of the initial Gaussian temperature distribution is taken equal to 14,000 K instead of 300 K.

3) The nozzle mass flow rate is adjusted to each set of conditions (p_0, W) according to the experimental data (only for defining the entrance velocity in the calculation area, for the SIMPLE procedure). This mass flow rate can be calculated in two different ways. Experimentally, through mass conservation in the expansion chamber, it is given by the pumping speed of the vacuum system, and by the pressure in the expansion chamber [2], assuming that the gas at the pump inlet is thermalized at 300 K. It can also be obtained, with the calculation, by integrating the product $n^* v^*_{\mathrm{ax}} \mathrm{d}S$ over the whole nozzle area. These two results will be compared further.

A. Temperature, Density, and Velocity Maps

Temperature and velocity maps are calculated for each experimental point (p_0, W). Qualitatively, it is observed, as expected, that the plasma core moves toward the laser waist when the conditions become closer to threshold. Quantitatively, it is possible

Table 2 Values of different parameters characterizing some typical experimental cases

Pressure p_0, 10^5 Pa	Laser power W, W	Pressure p_1, Pa	Freezing distance z_{freeze}/D^*	Mach disk location z_M/D^*
7	0	15.0	*4*	*145*
2	385	2.5	*5.5*	*190*
3	385	3.5	*6*	*195*
4	330	4.5	*5*	*200*
4	220	5.5	*5*	*180*
6	360	8.8	*5*	*175*
6	250	10.0	*5*	*165*
8	330	17.0	*5*	*145*
8	275	17.0	*5*	*145*
8	165	19.0	*5*	*135*

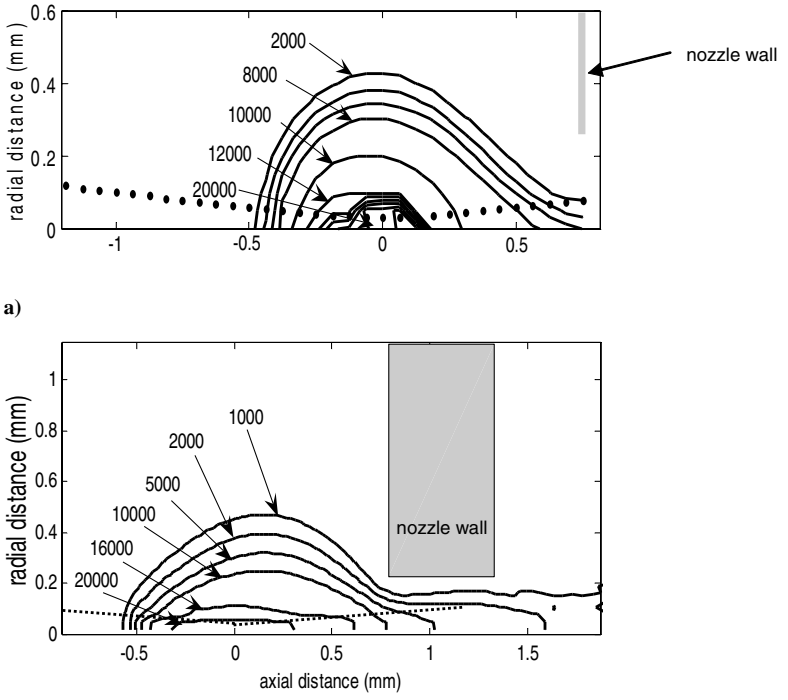

Fig. 6 Contour plot of the plasma temperature (in Kelvin) for a) SIMPLE and b) LCP;$p_0 = 3 \times 10^5$ Pa, $p_1 = 3.5$ Pa, $W = 330$ W.

to compare several results with the experimental data [30]: the axial temperature at the nozzle throat with the isentropic stagnation temperature [through Eq. (1)], the axial longitudinal velocity at the nozzle throat with the measured time-of-flight velocity [Eq. (2)], and the mass flow rate calculated at the nozzle with the flow rate given by the pumping speed of the vacuum system (and controlled by a flow meter). Most of the experimental data have been obtained previously [2,3].

Temperature maps are given in Fig. 6, for both calculation codes, mainly for the stagnation chamber. The laser beam profile is represented by a dotted line. The nozzle wall is shown by a shaded line in the SIMPLE case (Fig. 6a) and as a shaded area in the LCP case (Fig. 6b). It turns out that the extent of the plasma upstream of the nozzle is nearly the same with SIMPLE and LCP calculations. Figures 7a and 7b present contour maps for temperature and density, respectively, obtained with the LCP code, with more detail in the expansion chamber. In Fig. 7b, it should be noticed that the successive contour lines are separated by 1.5×10^{25} m^{-3} upstream of the nozzle throat, and 3×10^{23} m^{-3} in the expansion chamber. The freejet exhibits a very sudden expansion region clearly inscribed within a steep boundary which appears to be the lateral shock wave of the zone of silence.

B. Comparison Between Calculation and Experimental Data

1. Plasma Threshold

Experimentally, for a given focal length of the lens used and for a given distance between the laser waist and the nozzle throat, the plasma appears to be stable above a given line in the frame (p_0, W) and vanishes everywhere else [2,3,31]. The same finding is obtained with the calculations. In Fig. 8 are reported the lowest experimental points of operation (open circles). The error bars correspond to the mean square deviation over five measurements obtained by decreasing laser power at constant pressure p_0. For each calculation procedure, the shaded area represents the uncertainty on the calculated threshold. It is limited by the lowest stable line and by the highest unstable line which have been clearly obtained. Between these boundaries, the computation time becomes so long before the possible extinction of the plasma that it is quite difficult to assert whether the plasma is stable or not.

The agreement is remarkably good, for both calculations, for pressures higher than 3×10^5 Pa. Below this pressure, the LCP-FCT calculated thresholds do not follow the measured increase of the boundary below which no plasma exists. SIMPLE follows more or less the measured boundary. This effect could be explained by the assumptions on the C_p values. In the SIMPLE case, C_p is calculated

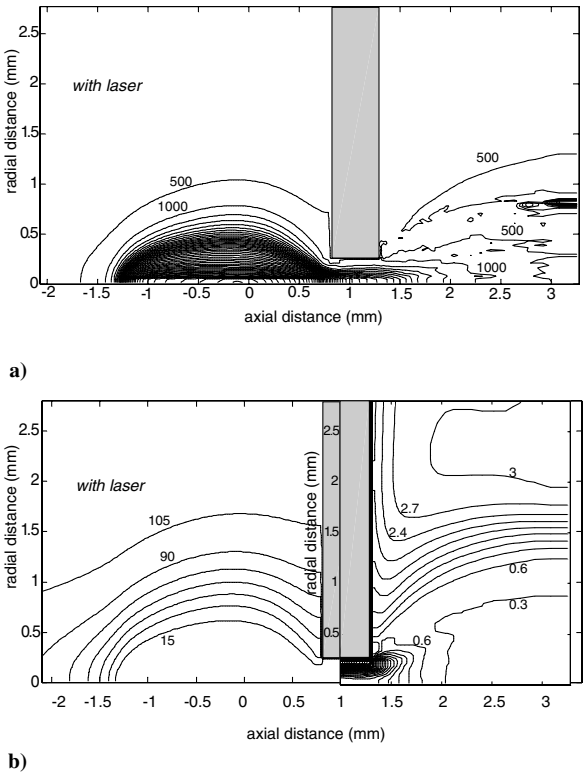

Fig. 7 Contour maps for a) temperature, and b) density, obtained from LCP calculation (units in Kelvin and 10^{24} m^{-3}, respectively); $p_0 = 4.5 \times 10^5$ Pa, $p_1 = 5.3$ Pa, $W = 360$ W.

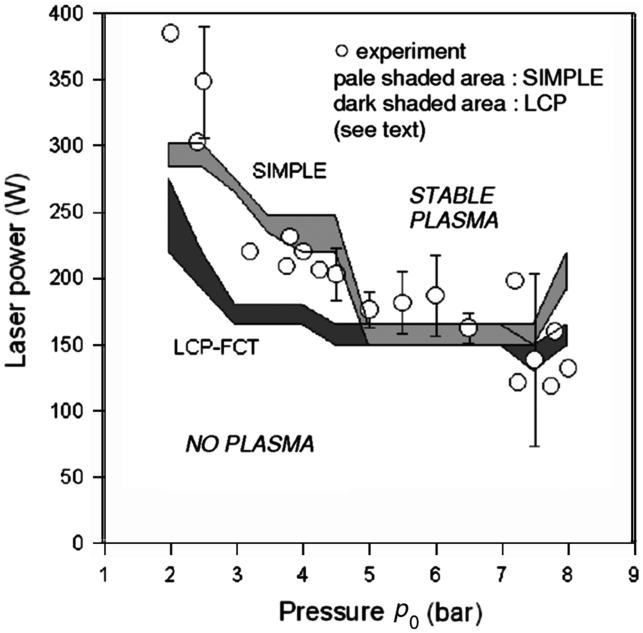

Fig. 8 Plasma threshold in terms of laser power and gas pressure.

as an approximation where the presence of Ar^{++} is neglected. This assumption appears especially valid for C_p at pressures higher than 1 bar, even at temperatures in the vicinity of 20,000 K [22]. In the present situation, lower pressures are achieved only in regions where the temperature decreases very quickly (in fact, only far downstream in the freejet), i.e., where Ar^{++} ions are not expected (and where the SIMPLE calculation is not carried out). And so, the C_p values are likely quite correct in the SIMPLE case. In counterpart, taking C_p as a constant is especially unrealistic at lower pressures [22], and this could be a reason for the threshold gap in the LCP case, for these lower pressures. Finally, a poorer balance between absorption coefficient and radiative loss could be possible at lower pressures. Perhaps the dependence of the radiative loss in terms of $p^{3/2}$ should be refined [21], or another formulation could be tested [13,32].

2. *Equivalent Stagnation Temperature*

The agreement between the experimental data and both calculations is generally good and remains within 20%, except on the boundaries of the stability region, close to threshold, where the error can reach 35%. Nevertheless, for the LCP-FCT calculation, the values obtained for the lowest laser power (165 W) are completely underestimated. These data are compared in Fig. 9 for three values of the laser power: one close to threshold (165 W), one far above threshold (360 W), and one intermediate value (275 W).

It appears, when reporting to the threshold data, that the threshold effect is less steep than for the experimental data, and appears rather as a slow decrease of plasma temperature than as a sudden plasma extinction. This could be the reason why the calculated temperatures are too small in the vicinity of the experimental threshold. The nonequilibrium model gives values of temperature significantly lower than the other data. Nevertheless, this model is the most promising for further improvements due to the large number of physical properties which are taken into account or which can be added.

3. *Axial Velocity*

There are two different ways for comparing the experimental data to the calculated values of the axial velocity. It is first possible to compare the final time-of-flight mean velocity with the velocity calculated at the nozzle throat, by means of Eq. (2). Also, for the LCP calculation, it is possible to compare directly the experimental velocity with the axial velocity obtained at the end of the continuous expansion.

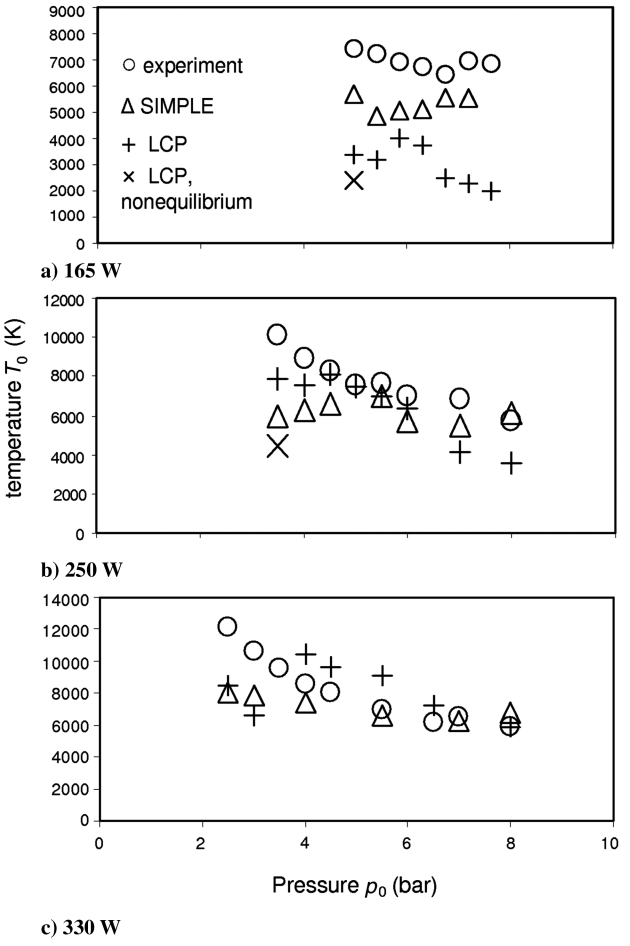

Fig. 9 Temperature T_0 as a function of gas pressure p_0 for different values of laser power.

These comparisons are made in Fig. 10, in the same conditions as in Fig. 9. In Figs. 9 and 10, the experimental error bars are approximately on the order of magnitude of the symbol size. As a matter of fact, the uncertainty on the measurement is small (for instance, in [2], the values of T_0 have been measured with an error bar of $\pm 0.5\%$ for a number of nozzle-skimmer distances); the possible error can only be due to a small shift of pressure and/or nozzle diameter during the acquisition time. Some of the data for the velocities reproduced in Fig. 10 are correlated with the corresponding T_0 values of Fig. 9. The experimental values of T_0, $T_{//\infty}$ ($\approx T$, the terminal translational temperature [1]), and v_∞ are connected by the adiabatic relation [Eq. (3)], which can be rewritten as $v_\infty^2 = a\,(T_0 - T)$, with $a = 1032.93$ in mks units. In the SIMPLE calculation, the sonic condition is imposed and v_∞ is determined by Eq. (2), and so, v_∞ and T_0 are connected by the same adiabatic law as the experimental data. For the LCP calculation, the sonic condition is not a preliminary prescription, and the adiabatic relation is subsidiary. Even when v_∞ is calculated from Eq. (2), v_{ax}^* is obtained from the calculation and is not directly correlated to T_0 (symbol + in Fig. 10). Then, it may be worth comparing the data with the results of Eq. (3). In this case, the correlation coefficient is found to be $a \approx 1250$ ($\approx$20% larger than the experimental value). When v_∞ is obtained directly from the calculation, at the end of expansion [symbol (米) in Fig. 10], there is no requisite at all between v_∞ and T_0. Then, the values of a are, respectively, for laser powers of 165, 250, and 330 W: 833 ± 100, 716 ± 40, 785 ± 40, i.e., respectively, 20%, 30%, and 25% lower than the experimental value. This means that the calculated velocity decreases too much during the expansion, but the main discrepancy, observed in the vicinity of the plasma threshold (for instance for $W = 165$ W), arises from an underestimation of T_0 and not from an inconsistency in the expansion description. Changing the value of γ, as proposed in [33],

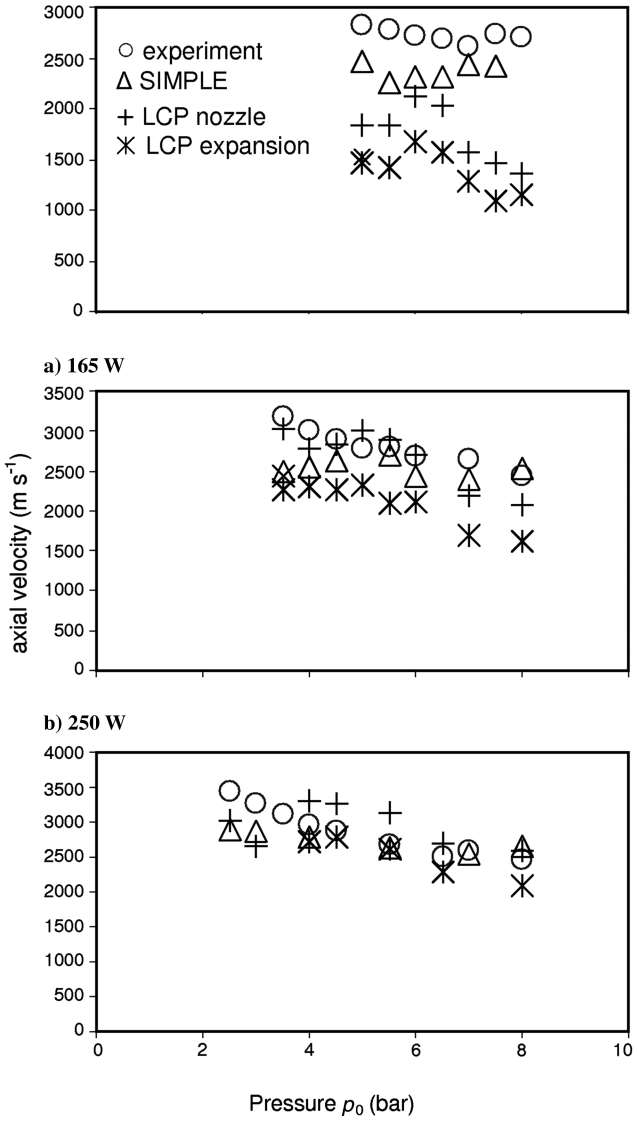

Fig. 10 Same as Fig. 9 for the axial velocity v_∞.

from 5/3 to 1.3, would lead to $a = 2480$ (+140%), and does not seem adequate in the present case, where the discrepancies remain within a reasonable range in most of the experimental conditions. The relative error between the LCP velocity values (values + of Fig. 10), and the experimental data (independent of γ) are summarized in Fig. 11 in the part of the plane (p_0, W) accessible to the experiment. Except for the lowest values of laser power, the accuracy is better than $\pm 20\%$.

As for the standard cold gas test calculation, it turns out that for the LCP calculation, the velocity obtained at the end of the freejet [values (✳) of Fig. 10] is, generally, on the same order of magnitude than the result of Eq. (2), but always significantly lower. This could be due to the limitation of the expansion region in the calculation.

4. Mass Flow Rate

The flow rate, integrated over the whole area of the nozzle throat, can be compared with the experimental flow rate, as deduced from the pumping conditions in the expansion chamber, assuming that the gas is thermalized at room temperature at the pumping flange (the mean free path is on the order of 0.5 mm at a pressure of about 10 Pa). The data are reported in Fig. 12, in which the full line represents the ideal case where the calculated flow rate would be equal to the experimental flow rate. The orders of magnitude are generally quite correct. For the SIMPLE procedure, the flow rates are always higher

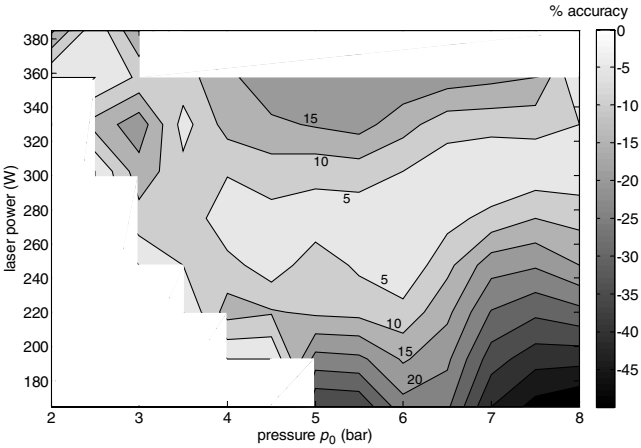

Fig. 11 Relative accuracy between velocities calculated with LCP through Eq. (2), and the experimental values.

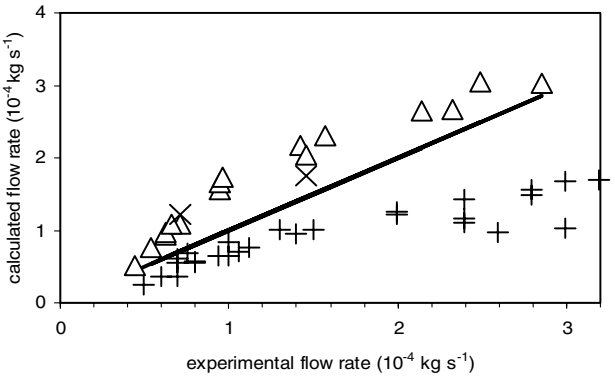

Fig. 12 Comparison between mass flow rate values, obtained from the different calculations, with the corresponding experimental values (same symbols as in Fig. 9).

than the experimental values, but the agreement becomes very good for the lowest and for the highest flow rates; the average error is 45%. For the LCP equilibrium calculation, the values are all lower than the experimental data, with a close agreement for the lowest flow rates (the average error is 33% below 1.6×10^{-4} kg/s), and an increasing discrepancy as the flow rate increases (50% above 1.6×10^{-4} kg/s). The average error is 38% on the complete range. It can be expected that the error on the experimental measurement is lower than $\pm 5\%$, as it is corroborated by three different means: two different vacuum gauges for the determination of p_1, and one flow meter on the gas inlet. And so, the LCP calculation is likely responsible for an underestimation of the highest flow rates, which are obtained with higher pressures and/or lower temperatures T_0; this range corresponds roughly to the maximum uncertainty region of the velocities.

IX. Discussion and Conclusions

The generating conditions of a laser-sustained plasma freejet have been simulated by two different numerical procedures (SIMPLE and LCP-FCT), and two different models (equilibrium and non-equilibrium cases). It turns out that the flowfield can be completely and accurately described, from the inlet conditions to the end of the expansion. And so, it is possible to predict the different possibilities of a fast atom beam generator, based on this principle, thus avoiding long and heavy experimental measurements. The LCP-FCT procedure appears as very efficient, with a good accuracy in the complete domain. Nevertheless, for the threshold predictions, the SIMPLE procedure gives better results, and also reveals a better behavior in conditions close to threshold. An extension of the LCP calculation including the complete description of the ignition of the

plasma (nonequilibrium model) could be applied to gas mixtures. Up to now, it has been used with the species Ar, Ar^+, and electrons, for pure argon. The addition of O_2, O_2^+, O, and O^+ should allow the conditions of an oxygen atom beam source [4,5] to be theoretically predicted. Finally, it can be noted that the pretty good agreement between the velocity calculated in the final stages of the freejet and the velocity deduced from Eq. (2) confirms the validity of the isentropic assumption for the expansion, with $\gamma = 5/3$, in the present plasma jet conditions. This seems consistent with a very low ionization degree in the expansion.

References

[1] Miller, D. R., "Free Jet Sources," *Atomic and Molecular Beam Methods*, edited by G. Scoles, Oxford Univ. Press, New York, 1988, pp. 14–53.

[2] Girard, J. M., Lebéhot, A., and Campargue, R., "Generating Conditions of a Laser-Sustained Argon Plasma Jet," *Journal of Physics D: Applied Physics*, Vol. 26, No. 9, 1993, pp. 1382–1393.

[3] Lebéhot, A., and Campargue, R., "Properties of an Argon Plasma Free Jet Generated from a Continuous Optical Discharge," *Physics of Plasmas*, Vol. 3, No. 7, 1996, pp. 2502–2510.

[4] Lebéhot, A., Kurzyna, J., Lago, V., Dudeck, M., and Nishida, M., "Simple Model for the Electronic Relaxation during the Expansion of a Plasma Generated in an Ar-O_2 Mixture," *Physics of Plasmas*, Vol. 6, No. 12, 1999, pp. 4750–4758.

[5] Lebéhot, A., Kurzyna, J., Lago, V., Dudeck, M., and Campargue, R., "Laser Sustained Plasma Free Jet and Energetic Atom Beam of Pure Argon or Oxygen Seeded Argon Mixture," *Atomic and Molecular Beams, The State of the Art 2000*, edited by R. Campargue, Springer, Berlin, 2001, pp. 237–251.

[6] Mertogul, A. E., and Krier, H. "Two-Temperature Modeling of Laser Sustained Hydrogen Plasmas," *Journal of Thermophysics and Heat Transfer*, Vol. 8, No. 4, 1994, pp. 781–790.

[7] Ashkenas, H., and Sherman, F. S., "Structure and Utilization of Supersonic Free Jets in Low Density Wind Tunnels," *Rarefied Gas Dynamics*, edited by J. H. De Leeuw, Academic Press, New York, 1966, pp. 84–105.

[8] Raizer, Y. P., "Optical Discharges," *Soviet Physics Uspekhi*, Vol. 23, No. 11, 1980, pp. 789–806.

[9] Patankar, S. V., "Calculation Procedure for Two-Dimensional Elliptic Situations," *Numerical Heat Transfer*, Vol. 4, Oct.–Dec. 1981, pp. 409–425.

[10] Oran, E. S., and Boris, J. P., *Numerical Simulation of Reactive Flow*, Elsevier, New York, 1987.

[11] Jeng, S. M., and Keefer, D. R., "Theoretical Investigation of Laser-Sustained Argon Plasmas," *Journal of Applied Physics*, Vol. 60, No. 7, 1986, pp. 2272–2279.

[12] Keefer, D. R., "Laser Sustained Plasmas," *Laser induced plasmas and applications*, edited by L. J. Radziemski, and D. A. Cremers, Marcel Dekker, New York, 1989, pp. 169–206.

[13] Beulens, J. J., Milojevic, D., Schram, D. C., and Vallinga, P. M., "Two-Dimensional Nonequilibrium Model of Cascaded Arc Plasma Flows," *Physics of Fluids B*, Vol. 3, No. 9, 1991, pp. 2548–2557.

[14] Surzhikov, S. T., "Laser-Plasma Generator with Artificial Turbulence of the Input Gas Stream," *Journal of Thermophysics and Heat Transfer*, Vol. 15, No. 2, 2001, pp. 239–242.

[15] Komurasaki, K., Arakawa, Y., Hosoda, S., Katsurayama, H., and Mori, K., "Fundamental Researches on Laser Powered Propulsion," AIAA Paper 2002-2200, May 2002.

[16] Szymanski, Z., "Effects of Beam Intensity Profile and Optics on Laser-Sustained Argon Plasma," *Journal of Physics D: Applied Physics*, Vol. 25, No.3, 1992, pp. 413–416.

[17] Girard, J. M., Lebéhot, A., and Campargue, R., "Numerical Simulation for the Generating Conditions of a Laser-Sustained Argon Plasma Jet," *Journal of Physics D: Applied Physics*, Vol. 27, No. 2, 1994, pp. 253–262.

[18] Johnston, T. W., and Dawson, J. M., "Correct Values for High-Frequency Power Absorption by Inverse Bremmstrahlung in Plasmas," *Physics of Fluids*, Vol. 16, No. 5, 1973, p. 722.

[19] Parisse, J. D., "Modélisation et simulation numérique de l'interaction laser-matière," Ph.D. Thesis, Univ. de Provence Aix-Marseille, Marseille, France, 2000.

[20] Zeitoun, D. E., and Parisse, J. D., "Modeling of Plasma Creation and Expansion Induced by a 193 Nanometer Laser," AIAA Paper 2001-2731, June 2001.

[21] Jeng, S. M., Keefer, D. R., Welle, R., and Peters, C., "Numerical Study of Laser-Sustained Argon Plasmas in a Forced Convective Flow," AIAA Paper 86-1078, May 1986.

[22] Matsuzaki, R., "Analytical Expressions for Specific Heats and Isentropic Exponent of High Temperature Gases 1: Monatomic and Diatomic Gases," *Japanese Journal of Applied Physics*, Vol. 21, No. 7, 1982, pp. 1003–1008.

[23] Chen, W. L. T., Heberlein, J., and Pfender, E., "Critical Analysis of Viscosity Data of Thermal Argon Plasmas at Atmospheric Pressure," *Plasma Chemistry and Plasma Processing*, Vol. 16, No. 4, 1996, pp. 635–650.

[24] Amic, K., "Oxygène Atomique dans les Conditions de l'Environnement Spatial: Expériences et Simulations d'une Source Entretenue par Laser," Ph.D. Thesis, Univ. d'Orléans, Orléans, France, 2006.

[25] Anderson, J. B., "Molecular Beams from Nozzle Sources," *Molecular Beams and Low Density Gas Dynamics*, edited by P. P. Wegener, Marcel Dekker, New York, 1974, pp. 1–91.

[26] Beylich, A. E., "Structure and Applications of Jets," *Rarefied Gas Dynamics*, edited by R. Brun, R. Campargue, R. Gatignol, and J. C. Lengrand, Cépaduès Editions, Toulouse, France, 1999, pp. 553–566.

[27] Beijerinck, H. C. W., and Verster, N. F., "Absolute Intensities and Perpendicular Temperatures of Supersonic Beams of Polyatomic Gases," *Physica*, Vol. 111C, Nos. 2–3, 1981, pp. 327–352.

[28] Anderson, J. B., and Fenn, J. B., "Velocity Distributions in Molecular Beams from Nozzle Sources," *Physics of Fluids*, Vol. 8, No. 5, 1965, pp. 780–787.

[29] Campargue, R., and Breton, J. P., "*Amélioration de la méthode des jets moléculaires supersoniques par augmentation simultanée des pressions génératrice et résiduelle*," Vol. 42, Entropie, Nov.–Dec. 1971, pp. 18–28 (in French).

[30] Amic, K., Parisse, J. D., Lebéhot, A., and Campargue, R., "Laser Sustained Plasma Free Jet for the Generation of Fast Atom Beam of Interest in the Simulation of Low Earth Orbit Environment," *25th International Symposium on Rarefied Gas Dynamics*, American Inst. of Physics Paper 3155, 2006.

[31] Moody, C. D., "Maintenance of a Gas Breakdown in Argon Using 10.6-μ cw Radiation," *Journal of Applied Physics*, Vol. 46, No. 6, 1975, pp. 2475–2482.

[32] Wilbers, A. T. M., Beulens, J. J., and Schram, D. C., "Radiative Energy Loss in a Two-Temperature Argon Plasma," *Journal of Quantitative Spectroscopy and Radiative Transfer*, Vol. 46, No. 5, 1991, pp. 385–392.

[33] Schram, D. C., Mazouffre, S., Engeln, R., and van de Sanden, M. C. M., "Physics of Plasma Expansion," *Atomic and Molecular Beams, The State of the Art 2000*, edited by R. Campargue, Springer, Berlin, 2001, pp. 209–235.